Available online at www.sciencedirect.com
ScienceDirect
Trans. Nonferrous Met. Soc. China 29(2019) 1583−1591
Transactions of Nonferrous Metals Society of China
www.tnmsc.cn

# Microstructure evolution and mechanical properties of Al−6.5Cu−0.6Mn−0.5Fe alloys with different Si additions

Rui XU[1], Bo LIN [1], Hao-yu LI [1], Hua-qiang XIAO[1], Yu-liang ZHAO[2], Wei-wen ZHANG[3]

1. School of Mechanical Engineering, Guizhou University, Guiyang 550025, China;
2. School of Mechanical Engineering, Dongguan University of Technology, Dongguan 523808, China;
3. School of Mechanical and Automotive Engineering,
South China University of Technology, Guangzhou 510640, China

Received 13 November 2018; accepted 5 June 2019

**Abstract:** The effect of Si content on the microstructures and mechanical properties of the heat-treated Al−6.5Cu−0.6Mn−0.5Fe alloy was investigated using image analysis, scanning electron microscopy (SEM), transmission electron microscopy (TEM), and tensile testing. The results show that the mechanical properties of Al−6.5Cu−0.6Mn−0.5Fe alloys decrease slightly when the Si content is below 1.0%. This can be attributed to the comprehensive effect of microstructure evolution, including the increase of nano-sized $\alpha$-Fe, the coarsened grain size, and an increase in $Al_2Cu$ content at the grain boundary. When the Si content is 1.5%, the mechanical properties of the Al−6.5Cu−0.6Mn−0.5Fe alloys decrease significantly, and this can be attributed to the agglomerated second intermetallics, which is resulted from the formation of excess Si particles.
**Key words:** Al−Cu alloys; iron-rich intermetallics; Si; tensile properties

## 1 Introduction

With the increasing requirements for environmental protection and green manufacturing, recycling Al alloys has become an important direction for development in the aluminum industry. However, recycled Al alloys contain many impurity elements, such as Fe, Si, Ni, Zn, Mg and Mn [1,2]. Iron is the most harmful impurity element in recycled aluminum alloys. Because the solid solubility of Fe in Al alloys is limited, Fe usually precipitates in the form of hard and brittle Fe-rich intermetallics, such as Chinese script $\alpha$-Fe ($Al_{15}(FeMn)_3(SiCu)_2$) [3], $Al_6(FeMn)$ [4], $Al_mFe$ [5], plate-like $Al_3(FeMn)$ [6], and $\beta$-Fe ($Al_7Cu_2Fe$) [7]. Several methods have been effectively used to prevent the detrimental effects of iron in aluminum alloys. These methods include (1) reducing the formation of Fe-rich intermetallics by lowering the Fe levels to be as low as economically possible, and (2) modifying the Fe-rich intermetallics using chemical or physical approaches. In the chemical approaches, Mn and Si elements are added to break up the needle-like intermetallics or to transform them into block or Chinese script. The physical approaches include the use of superheated melt, solidification under high cooling rate, and melt treatment [8−11].

Al−Cu alloys are widely used in aerospace and automobile manufacturing industry because of their excellent fatigue properties, high specific strength, and good heat resistance. However, Al−Cu alloys have poor casting properties, such as hot cracking susceptibility and fluidity in cast aluminum alloys [12]. It has been found that Si and Cu alloying of Al−Cu alloys decreases hot cracking susceptibility [13−15]. SABAU et al [15] found that Al−Cu alloys have the lowest thermal cracking tendency when the copper content is 7.3% and 8%. In our previous work, we found that nano-sized $\alpha$-Fe can be formed in Al−Cu alloys that have high Cu and Fe content, and this significantly improves the mechanical

**Foundation item:** Projects (51704084, 51605106) supported by the National Natural Science Foundation of China; Project (2017M623068) supported by China Postdoctoral Science Foundation; Project (2015A030312003) supported by the Natural Science Foundation for Team Research of Guangdong Province, China; Project (JC(2016)1026)) supported by the Science and Technology Foundation of Guizhou Province of China; Project (KY(2017)101)) supported by the Young Talent Growth Foundation of Education Department of Guizhou Province of China; Project (RC2017(5788)) supported by the Science and Technology Plan of Guizhou Province of China
**Corresponding author:** Bo LIN; Tel/Fax: +86-851-83627516; E-mail: linbo1234@126.com
DOI: 10.1016/S1003-6326(19)65065-X

properties [16]. The nano-sized $\alpha$-Fe phase is commonly observed in 3xxx and 6xxx alloys with high Si content [17,18]. Therefore, it can be expected that adding Si will promote the formation of the nano-sized $\alpha$-Fe phase in Al−Cu alloys. Also, Si content has a significant effect on the formation of Fe-rich intermetallics. However, Si is also an impurity element in Al−Cu alloys. As a result, the Si content is usually limited to below 0.1% for high-performance Al−Cu alloys [19]. However, strictly controlling the Si content in aluminum alloys will make these alloys expensive and is not conducive to the recycling of waste aluminum. Therefore, the effects of different Si contents on the microstructure and properties of the Al−6.5Cu−0.6Mn−0.5Fe alloy were studied for the purpose of promoting the efficient use of recycled aluminum.

## 2 Experimental

Experimental alloys with different Si contents were prepared using commercially pure Al (99.5%), Al−50%Cu, Al−10%Mn, Al−20%Si and Al−5%Fe master alloys. The compositions of the alloys were determined using optical emission spectrometry, and the results are listed in Table 1. First, pure Al, Al−5%Fe and Al−20%Si master alloys were preheated in a clay-graphite crucible using an electric resistance furnace at 400 °C for 1 h to eliminate water vapor. The raw materials were then melted at 730 °C. Al−50%Cu and Al−10%Mn master alloys were added at 730 °C. Finally, the temperature of the melt was maintained at 730 °C for 30 min. Approximately 10 kg of the melts were degassed using argon to minimize the hydrogen content. The melt was then poured into a cylindrical die, which had a size of 80 mm in height and 50 mm in diameter. The die temperature was set to be 250 °C, and the pouring temperature was 730 °C. T7 heat treatment conditions were used in this study to stabilize the microstructures. The samples were then solution-treated at 535 °C for 12 h before being quenched in warm water at 100 °C. The samples were then aged using T7 conditions at 215 °C for 16 h. For mechanical tests, samples with a diameter of 10 mm and a height of 80 mm were produced using a wire electrical discharge machining. The tensile test was carried out on an MTS CMT5105 standard testing machine, and the reported values are the averages of at least three samples. Samples for the micro-hardness test and metallographic observation were cut in the gauge length part from selected tensile specimens. The location for the micro-hardness test was restricted to the center of the $\alpha$(Al) dendrite near the center of the etched specimens. The micro-hardness was measured on a tester equipped with a Vickers diamond indenter using an indentation load of 100 g. The value reported is the average of more than 10 readings. The samples used for metallographic observations were etched in 0.5% HF solution for 30 s. The morphology, the Fe-rich phase, and the fracture surfaces were analyzed using SEM (Nova Nano SEM 430) attached with EDS. Precipitates in the $\alpha$(Al) matrix were analyzed using TEM (JEOL JEM−3010) at 200 kV. The area fraction of the intermetallics and precipitations of the alloys were quantitatively calculated by using image Pro Plus software.

**Table 1** Chemical composition of alloy (wt.%)

| Alloy | Cu | Mn | Fe | Si | Al |
|---|---|---|---|---|---|
| Al−6.5Cu−0.6Mn−0.5Fe−0Si (0Si) | 6.45 | 0.66 | 0.55 | 0.04 | Bal. |
| Al−6.5Cu−0.6Mn−0.5Fe−0.5Si (0.5Si) | 6.47 | 0.62 | 0.54 | 0.58 | Bal. |
| Al−6.5Cu−0.6Mn−0.5Fe−1.0Si (1.0Si) | 6.50 | 0.63 | 0.53 | 1.13 | Bal. |
| Al−6.5Cu−0.6Mn−0.5Fe−1.5Si (1.5Si) | 6.52 | 0.63 | 0.56 | 1.50 | Bal. |

## 3 Results

### 3.1 Microstructure of as-cast alloys

Figure 1 shows the microstructure of the as-cast Al−6.5Cu−0.6Mn−0.5Fe alloy with different Si contents. Table 2 gives EDS data of the Fe-rich phase in the as-cast Al−6.5Cu−0.6Mn−0.5Fe alloy with different Si contents. The Fe-rich phase shows Chinese script morphology in all of the experimental alloys. As seen in Table 2, the Chinese script Fe-rich intermetallic is $\alpha$-Fe ($Al_{15}(FeMn)_3Cu_2$ or $Al_{15}(FeMn)_3(CuSi)_2$) [3,9]. In addition, the amount of Si in $\alpha$-Fe increases with an increase in Si content, and this is because the Al atom is substituted by the Si atom in the Fe-rich phase [20]. On the basis of Fig. 1, the area fraction of $\alpha$-Fe is quantitatively calculated. The area fraction of $\alpha$-Fe increases from 3.9% to 4.3% and then to 4.5% when the Si content is increased from 0 to 0.5% and then to 1.0%. The results show that the area fraction of $\alpha$-Fe increases with an increase in the Si content, and this is similar to the results reported in the work by LIU et al [10].

### 3.2 Microstructure of heat-treated alloys

Figure 2 shows the microstructure of the heat-treated Al−6.5Cu−0.6Mn−0.5Fe alloy with different Si contents. Table 3 gives EDS data of the Fe-rich phase in the heat-treated Al−6.5Cu−0.6Mn−0.5Fe alloy with different Si contents. Compared with the as-cast alloy, $Al_2Cu$ is completely dissolved into the $\alpha$(Al) matrix after the T7 heat treatment in the 0Si alloy. Also, Cu-rich $\beta$-Fe transforms from $\alpha$-Fe after solution heat treatment in the 0Si alloy. The amount of $Al_2Cu$ increases, and $\alpha$-Fe

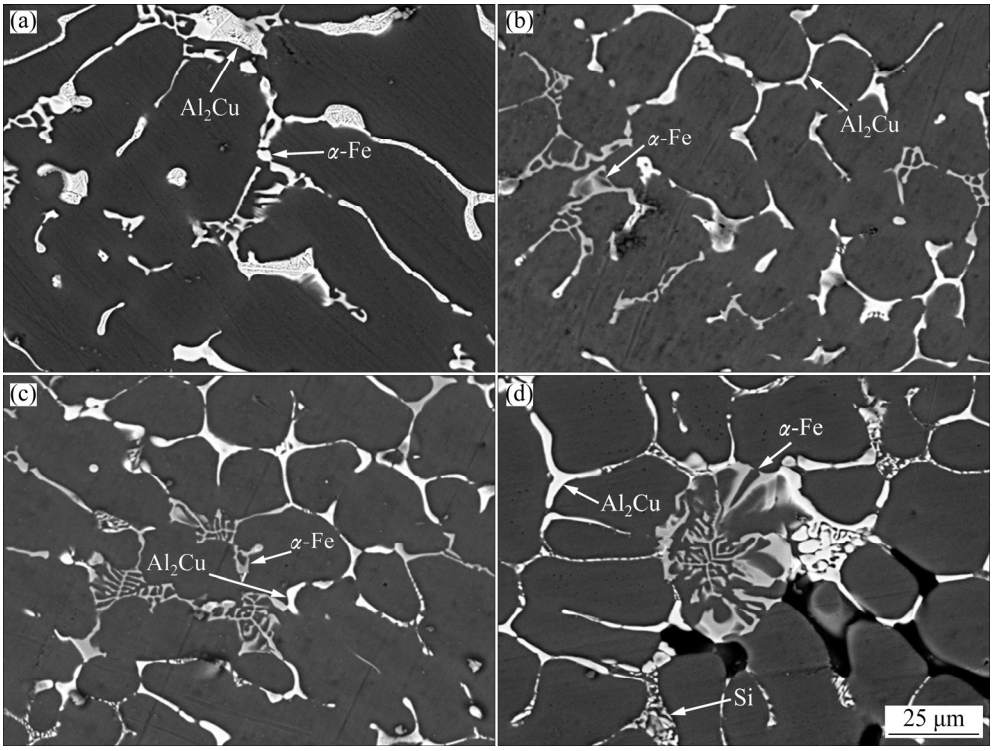


**Fig. 1** Microstructures of as-cast Al−6.5Cu−0.6Mn−0.5Fe alloys with different Si contents: (a) 0Si; (b) 0.5Si; (c) 1.0Si; (d) 1.5Si

**Table 2** Compositions of Fe-rich intermetallics in as-cast condition (at.%)

| Alloy | Phase | Al | Cu | Mn | Fe | Si |
|---|---|---|---|---|---|---|
| 0Si | *α*-Fe | 78.99±2.06 | 8.62±2.05 | 4.22±0.61 | 8.17±1.92 | − |
| 0.5Si | *α*-Fe | 77.71±0.72 | 3.59±0.37 | 3.41±0.24 | 7.00±0.44 | 8.28±0.19 |
| 1.0Si | *α*-Fe | 74.70±2.42 | 2.67±0.29 | 5.48±1.04 | 8.08±0.93 | 9.07±1.56 |
| 1.5Si | *α*-Fe | 73.30±1.92 | 4.25±2.48 | 4.50±2.09 | 10.55±1.92 | 7.41±0.88 |

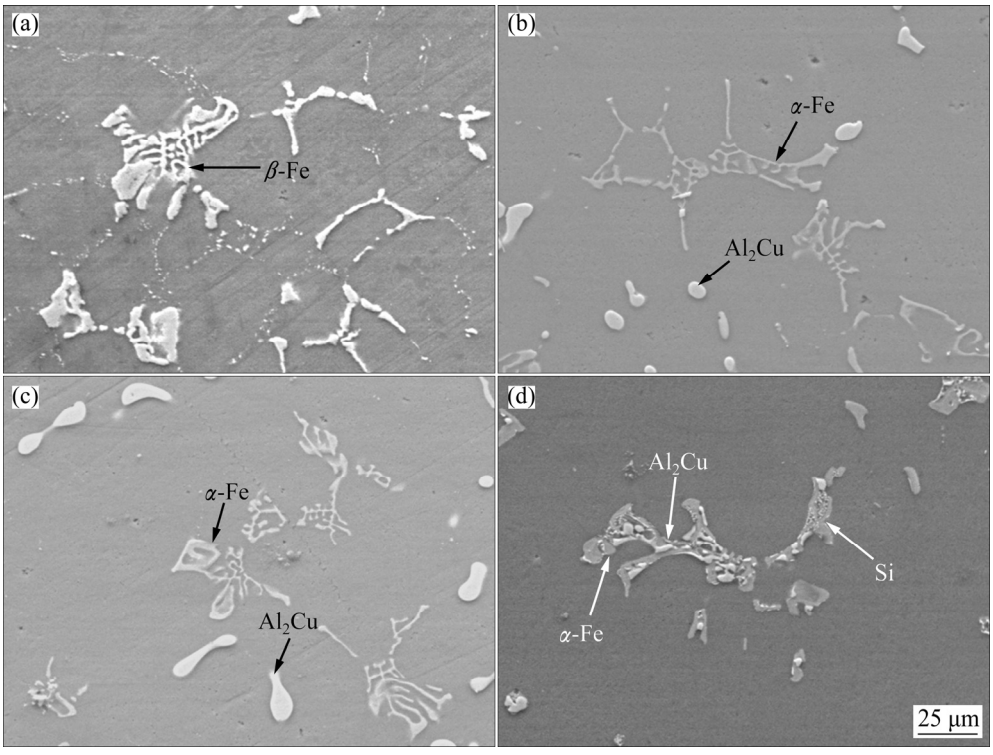


**Fig. 2** Microstructures of heat-treated Al−6.5Cu−0.6Mn−0.5Fe alloys with different Si contents: (a) 0Si; (b) 0.5Si; (c) 1.0Si; (d) 1.5Si

remains with an increase of the Si content. With a further increase in the amount of added Si to 1.5%, Si particles appear in the alloys. Also, excessive Si particles agglomerate with the $\beta$-Fe phase and $Al_2Cu$ phase at the grain boundary.

Figure 3 shows the effects of different Si contents on the grain size of the Al−6.5Cu−0.6Mn−0.5Fe alloy. The grain size of the alloy increases with an increase in the Si content. The grain sizes of alloys with different Si contents are quantitatively analyzed, and the results are shown in Fig. 3(f). The grain size of the 0Si alloy is estimated to be 540 μm, much less than that of the 1.5Si alloy (2350 μm).

Figure 4 shows the morphology and EDS data of the second phase in the $\alpha$(Al) matrix with different Si contents. According to EDS result of the 0.5Si alloy, the second phase precipitations in the $\alpha$(Al) matrix are $T$ phase and $\alpha$-Fe. Furthermore, the amount of $T$ phase

**Table 3** Compositions of Fe-rich intermetallics in heat-treated condition (at.%)

| Alloy | Phase | Al | Cu | Mn | Fe | Si |
|---|---|---|---|---|---|---|
| 0Si | $\beta$-Fe | 73.82±2.51 | 17.78±1.80 | 2.09±0.02 | 6.32±0.70 | − |
| 0.5Si | $\alpha$-Fe | 74.15±0.75 | 4.52±0.43 | 4.66±0.19 | 8.13±1.29 | 8.54±0.19 |
| 1.0Si | $\alpha$-Fe | 70.25±2.91 | 4.07±0.22 | 5.57±0.51 | 9.17±1.46 | 10.94±2.00 |
| 1.5Si | $\alpha$-Fe | 71.47±1.54 | 3.23±0.63 | 6.12±0.81 | 7.64±0.68 | 11.54±1.23 |

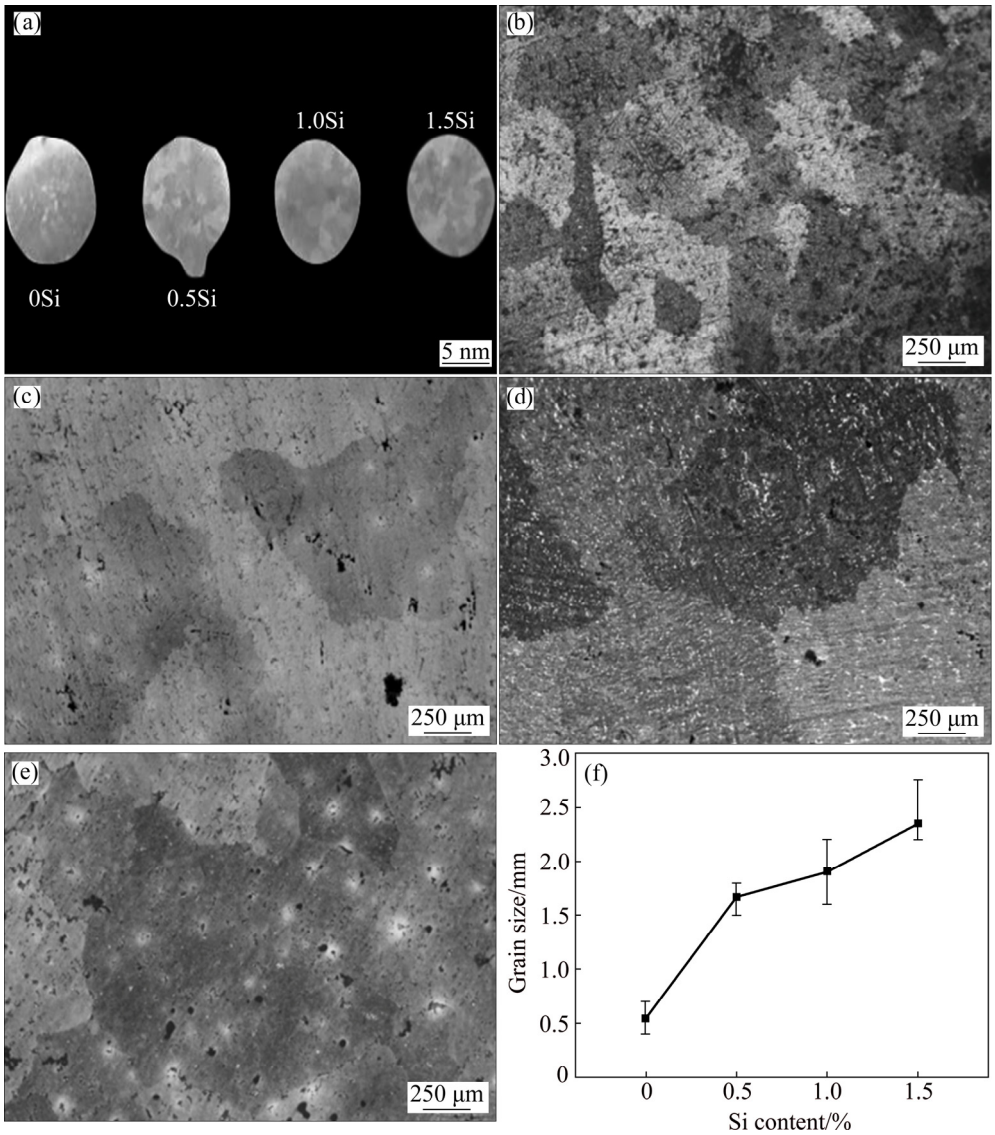


**Fig. 3** Macro-etched cross-section morphology of samples (a), micro-images of grain size for 0Si (b), 0.5Si (c), 1.0Si (d) and 1.5Si (e) alloys, and quantitatively-analyzed grain sizes (f)

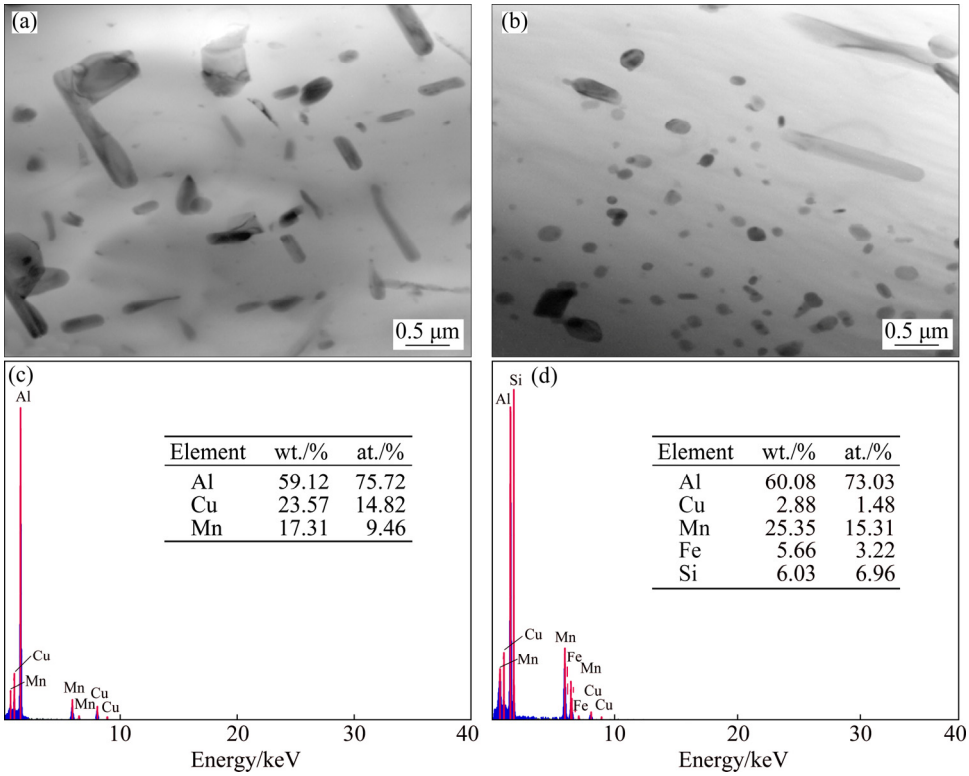


**Fig. 4** TEM images (a, b) and EDS results (c, d) of alloys with different Si contents: (a, c) 0Si; (b, d) 0.5Si

decreases and that of $\alpha$-Fe increases in alloys with an increase in Si content. This indicates that adding Si promotes the formation of the $\alpha$-Fe phase in the $\alpha$(Al) matrix. These results are also consistent with the previous finding that adding Si promotes the formation of the $\alpha$-Fe phase during T7 heat treatment in the 3xxx and 6xxx alloys [17,18]. On the basis of Fig. 4, the area fractions of $T$ phases and $\alpha$-Fe phases are quantitatively calculated. The area fractions of $T$ phases and $\alpha$-Fe phases in the 0Si alloy are 12.6% and 1.3%, respectively. And, the area fractions of $T$ phases and $\alpha$-Fe phases in the 0.5Si alloy are 5.9% and 10.2%, respectively. These results further prove that the Si content promotes the formation of the $\alpha$-Fe phase in the $\alpha$(Al) matrix.

Figure 5 shows micro-hardness of alloys with different Si contents. Adding Si obviously increases the micro-hardness of the matrix. The micro-hardness of the 0Si alloy (about HV 92.7) is much lower than that of the 1.0Si alloy (about HV 110.5). These results can be attributed to the increase in the amount of nano-sized $\alpha$-Fe phase with Si addition.

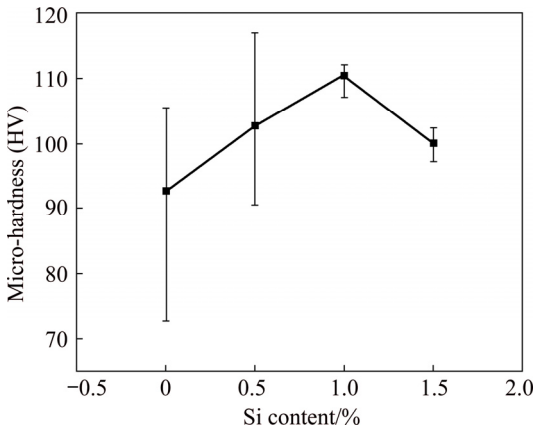


**Fig. 5** Micro-hardness of alloy with different Si contents

### 3.3 Mechanical properties of alloys

Figure 6 shows the mechanical properties of the heat-treated Al−6.5Cu−0.6Mn−0.5Fe alloy with different Si contents. The strength and elongation decrease as the Si content is increased. The mechanical properties of the Al−6.5Cu−0.6Mn−0.5Fe alloys decrease slightly when the Si content is below 1.0%. The ultimate tensile

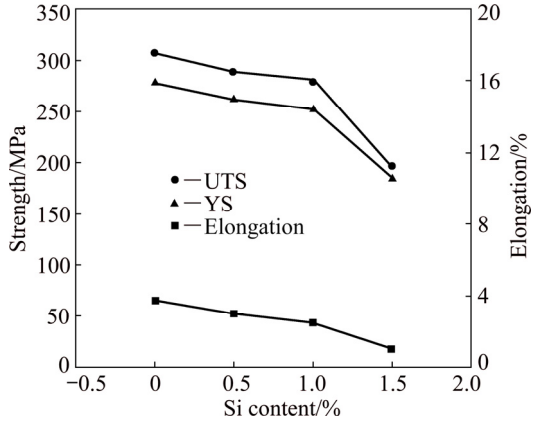


**Fig. 6** Mechanical properties of Al−6.5Cu−0.6Mn−0.5Fe alloys with different Si contents

strength (UTS), yield strength (YS), and elongation of the heat-treated 1.0Si alloy are recorded as 280 MPa, 253 MPa, and 2.5%, respectively. When the Si content is 1.5%, the mechanical properties of the Al−6.5Cu−0.6Mn−0.5Fe alloys decrease significantly, and this can be attributed to the precipitation of Si particles and the agglomeration of the coarse second phase.

### 3.4 Fracture surfaces of alloys

Figure 7 shows the fracture surfaces of alloys with different Si contents. There are some dimples on the fracture surfaces, and this indicates that the fractures of alloy exhibit certain ductile fracture characteristics. When the Si content is less than 1.0%, the alloy fracture surfaces are not significantly different, but when the Si content is 1.5%, brittle fracture characteristics become obvious. In addition, the morphology of the second phase of the alloys with different Si contents is obviously different on the fracture surfaces. When the Si content is 0%, there are some cracks in the cylindrical $\beta$-Fe ($Al_7Cu_2Fe$), and this indicates that $\beta$-Fe acts as crack initiation sites and leads to quasi-cleavage fracture (Fig. 7(a)). With a further increase in the Si content, cracks are also found in the $\alpha$-Fe and $Al_2Cu$ phases on the fracture surfaces, and this indicates that the brittle $\alpha$-Fe and $Al_2Cu$ act as potential cleavage initiators (Figs. 7(b, c)). However, the amount of cracks in $\alpha$-Fe is less than that in $\beta$-Fe, and this indicates that $\alpha$-Fe is less harmful than the cylindrical $\beta$-Fe [21]. In the 1.5Si alloys, the agglomerated second intermetallic phases are clearly seen when the fracture surfaces undergo cleavage fracture (Fig. 7(d)). The fracture surfaces clearly show that the plasticity of the alloy does not obviously change when the Si content is below 1.0%. However, the plasticity of the alloy decreases sharply with an increase in the Si content to 1.5%.

Figure 8 shows the longitudinal fracture morphology of alloys with different Si contents. When the Si content is 0%, there are many $\beta$-Fe phases on the fracture surface of the alloy. This indicates that the brittle $\beta$-Fe acts as potential cleavage initiators (Fig. 8(a)). With a further increase in the Si content (below 1.0%), the $\alpha$-Fe particles and the $Al_2Cu$ phase are observed at or beneath the fracture surface in the alloy, and this means that the $\alpha$-Fe particles and $Al_2Cu$ act as potential cleavage initiators (Figs. 8(b, c)). A large amount of agglomerated second intermetallics precipitate on the fracture surface of the 1.5Si alloy, and a crack of agglomerated second intermetallics results in the formation of secondary cracks (Fig. 8(d)).

## 4 Discussion

Figure 6 shows that the UTS, YS and elongation of the heat-treated alloy decrease with an increase in Si content, and this is mainly because of microstructure evolution.

First, adding Si promotes the transformation from $T$ ($Al_{20}Cu_2Mn_3$) phase to nano-sized $\alpha$-Fe after T7 heat treatment. This phenomenon can be explained by the Si

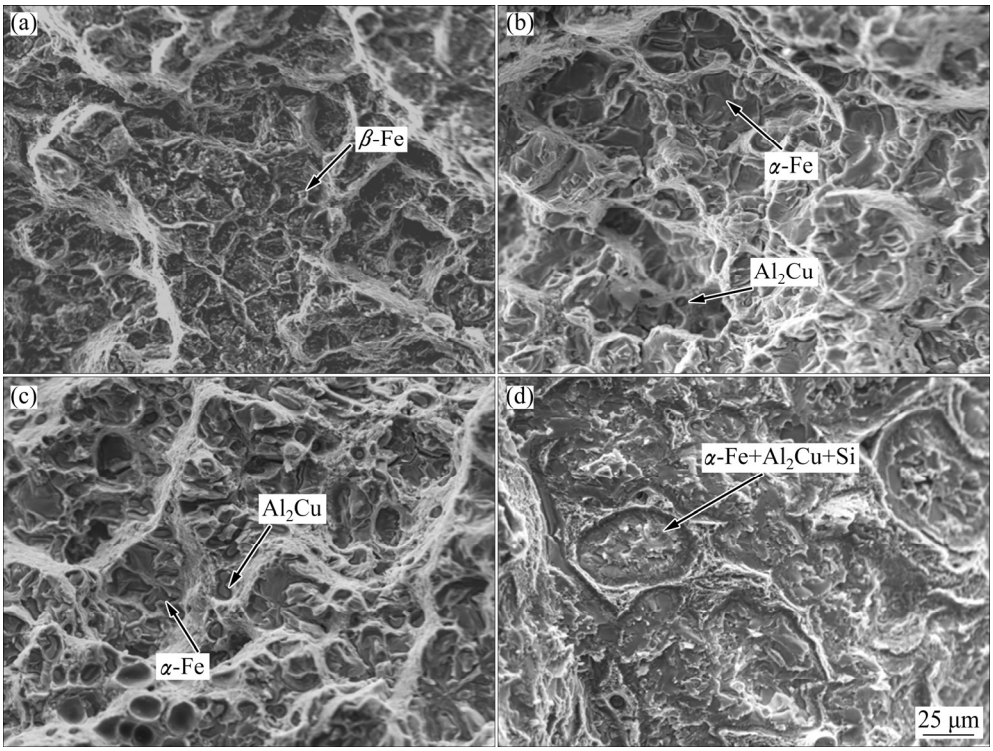


**Fig. 7** Fractographs of alloys with different Si contents: (a) 0Si; (b) 0.5Si; (c) 1.0Si; (d) 1.5Si

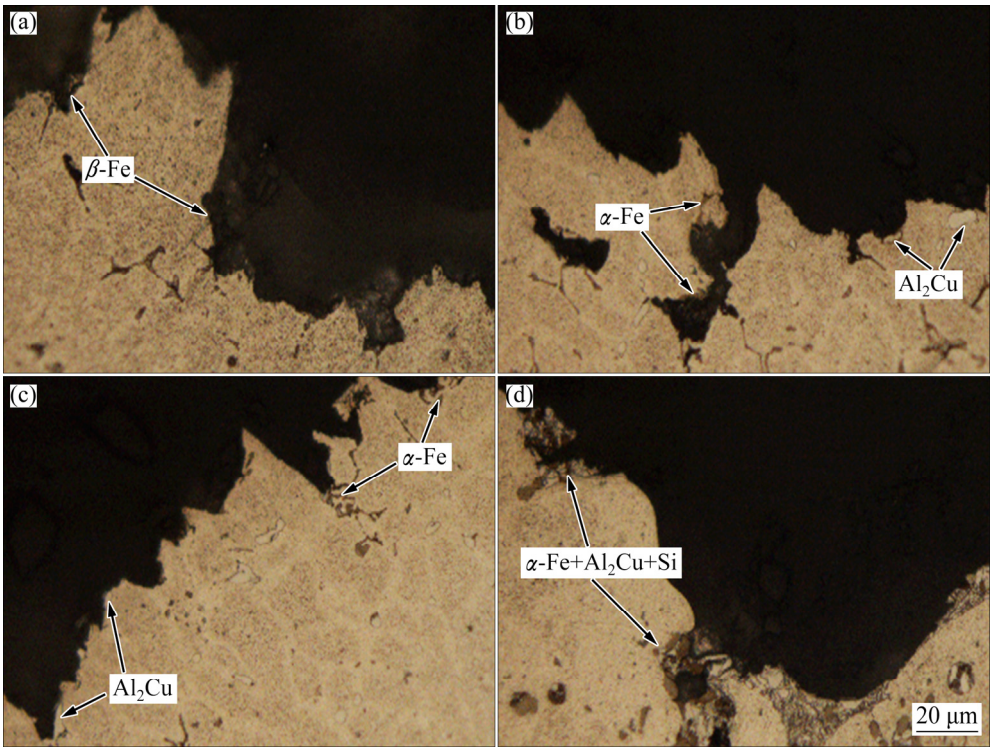


**Fig. 8** Longitudinal fracture morphologies of alloys with different Si contents: (a) 0Si; (b) 0.5Si; (c) 1.0Si; (d) 1.5Si

atom replacing the Al atom in the Fe-rich phase. As a result, adding Si promotes the formation of the $\alpha$-Fe phase [17,18]. This result is consistent with the previous finding that an increase in Si content can promote the formation of $\alpha$-Fe phase in the heat-treated 3xxx and 6xxx aluminum alloys. It has been reported that the formation of nano-sized $\alpha$-Fe phase is more beneficial than the large $T$ phase for the properties of alloys [22].

In addition, Si content obviously increases the grain size of alloys (Fig. 3). These results can be attributed to the decreased amount of $T$ phases in the matrix with an increase in Si content. Many researchers have reported that the $T$ phases prevent grain growth of Al−Cu alloys [8,23].

Finally, an increase in the Si content stabilizes $\alpha$-Fe and inhibits the transformation of $\alpha$-Fe to $\beta$-Fe during heat treatment. In Si-free alloys, $\alpha$-Fe transforms into copper-rich $\beta$-Fe ($(Al_{15}(FeMn)_3Cu_2 + 4Al_2Cu \rightarrow 3Al_7Cu_2(FeMn) + 2\alpha(Al)$) [20,24,25]. However, $\alpha$-Fe remains stable and reduces Cu consumption in alloys with high Si content, and this leads to an increase in the $Al_2Cu$ phase at the grain boundaries. The brittle $Al_2Cu$ phase acts as a potential cleavage initiator, and this indicates that an increase in the $Al_2Cu$ phase in alloys with high Si content deteriorates the performance of the alloy.

In conclusion, the decrease in mechanical properties can be attributed to the comprehensive effect of microstructure evolution, including an increase in nano-sized $\alpha$-Fe, the coarsened grain size, and an increase in $Al_2Cu$ at the grain boundary. When the Si content is 1.5%, the alloy properties decrease sharply because of excess Si particles and the agglomeration of brittle second intermetallics at the grain boundaries. These results demonstrate that the Si content should be appropriately controlled in the Al−Cu alloys. In this study, acceptable mechanical properties are achieved by controlling the Si content to be below 1.0%. Moreover, it is feasible to extend the Fe and Si contents for the purpose of using recycled aluminum alloys, which greatly reduces manufacturing costs. Also, an increase in nano-sized $\alpha$-Fe is beneficial to improving elevated mechanical properties [26−28]. Also, an increase in $Al_2Cu$ at the grain boundary is beneficial to improving elevated mechanical properties [29]. Therefore, it can be expected that the Al−6.5Cu−0.6Mn−0.5Fe alloy with high Si content will be beneficial to the mechanical properties at elevated temperature. Further work will be carried out to evaluate the mechanical properties at elevated temperature for industrial applications of Al−6.5Cu−0.6Mn−0.5Fe with high Si content.

## 5 Conclusions

(1) An increase in Si content in the Al−6.5Cu−0.6Mn−0.5Fe alloy promotes the transformation of the $T(Al_{20}Cu_2Mn_3)$ phase to nano-sized $\alpha$-Fe in the matrix. A decrease in the $T(Al_{20}Cu_2Mn_3)$ phase in alloys with high

Si content weakens the inhibition ability of grain growth, and this leads to coarsening of grain size.

(2) Adding Si stabilizes $\alpha$-Fe and inhibits the transformation from $\alpha$-Fe to $\beta$-Fe after heat treatment, and this leads to an increase in the $Al_2Cu$ phase in the alloy.

(3) Mechanical properties of the Al−6.5Cu−0.6Mn−0.5Fe alloy decrease with an increase in Si content. Mechanical properties of Al−6.5Cu−0.6Mn−0.5Fe alloys decrease slightly when the Si content is below 1.0%. However, the mechanical properties of Al−6.5Cu−0.6Mn−0.5Fe−1.5Si alloys decrease significantly. This can be attributed to the agglomerated second intermetallic that is resulted from the formation of excess Si particles.

## References


[1] BELOV N A, ESKIN D G, AKSENOV A A. Iron in aluminium alloys: Impurity and alloying element [M]. Florida, USA: CRC Press, 2014.

[2] ZHANG L F, GAO J W, DAMOAH L N W, ROBERTSON D G. Removal of iron from aluminum: A review [J]. Mineral Processing and Extractive Metallurgy Review, 2012, 33(2): 99−157.

[3] LIU K, CAO X, CHEN X G. Solidification of iron-rich intermetallic phases in Al−4.5Cu−0.3Fe cast alloy [J]. Metallurgical and Materials Transactions A, 2011, 42(7): 2004−2016.

[4] ZHANG W W, LIN B, LUO Z, ZHAO Y L, LI Y Y. Formation of Fe-rich intermetallic compounds and their effect on the tensile properties of squeeze-cast Al−Cu alloys [J]. Journal of Materials Research, 2015, 30(16): 2474−2484.

[5] LIU K, CAO X, CHEN X G. A new iron-rich intermetallic−$Al_mFe$ phase in Al−4.6Cu−0.5Fe cast alloy [J]. Metallurgical and Materials Transactions A, 2012, 43(4): 1097−1101.

[6] LIU K, CAO X, CHEN X G. Precipitation of iron-rich intermetallic phases in Al−4.6Cu−0.5Fe−0.5Mn cast alloy [J]. Journal of Materials Science, 2012, 47(10): 4290−4298.

[7] TSENG C J, LEE S L, WU T F, LIN J C. Effects of Fe content on microstructure and mechanical properties of A206 alloy [J]. Materials Transactions JIM, 2000, 41(6): 708−713.

[8] TSENG C J, LEE S L, TSAI S C, CHENG C J. Effects of manganese on microstructure and mechanical properties of A206 alloys containing iron [J]. Journal of Materials Research, 2002, 17(9): 2243−2250.

[9] KAMGA H K, LAROUCHE D, BOURNANE M, RAHEM A. Solidification of aluminum−copper B206 alloys with iron and silicon additions [J]. Metallurgical and Materials Transactions A, 2010, 41(11): 2844−2855.

[10] LIU K, CAO X, CHEN X G. Effect of Mn, Si, and cooling rate on the formation of iron-rich intermetallics in 206 Al−Cu cast alloys [J]. Metallurgical and Materials Transactions B, 2012, 43(5): 1231−1240.

[11] WANG Q L, GENG H R, ZHANG S, JIANG H W, ZUO M. Effects of melt thermal-rate treatment on Fe-containing phases in hypereutectic Al−Si alloy [J]. Metallurgical and Materials Transactions A, 2014, 45(3): 1621−1630.

[12] WANG L, WANG N, PROVATAS N. Liquid channel segregation and morphology and their relation with hot cracking susceptibility during columnar growth in binary alloys [J]. Acta Materialia, 2017, 126: 302−312.

[13] KAMGA H K, LAROUCHE D, BOURNANE M, RAHEM A. Hot tearing of aluminum–copper B206 alloys with iron and silicon additions [J]. Materials Science and Engineering A, 2010, 527(27−28): 7413−7423.

[14] KANG B K, SOHN I. Effects of cu and Si contents on the fluidity, hot tearing, and mechanical properties of Al−Cu−Si alloys [J]. Metallurgical and Materials Transactions A, 2018, 49(10): 5137−5145.

[15] SABAU A S, MIRMIRAN S, GLASPIE C, LI S, APELIAN D, SHYAM A, HAYNES J A, RODRIGUEZ A F. Hot-tearing assessment of multicomponent nongrain-refined Al−Cu alloys for permanent mold castings based on load measurements in a constrained mold [J]. Metallurgical and Materials Transactions B, 2018, 49(3): 1267−1287.

[16] LIN B, XU R, LI H Y, XIAO H Q, ZHANG W W, LI S B. Development of high Fe content squeeze cast 2A16 wrought Al alloys with enhanced mechanical properties at room and elevated temperatures [J]. Materials Characterization, 2018, 142: 389−397.

[17] ALEXANDER D T L, GREER A L. Solid-state intermetallic phase tranformations in 3XXX aluminium alloys [J]. Acta Materialia, 2002, 50(10): 2571−2583.

[18] BIROL Y. The effect of homogenization practice on the microstructure of AA6063 billets [J]. Journal of Materials Processing Technology, 2004, 148(2): 250−258.

[19] GREEN J A S. Aluminum recycling and processing for energy conservation and sustainability [M]. Ohio, USA: ASM International, 2007.

[20] KAMGA H K, LAROUCHE D, BOURNANE M, RAHEM A. Mechanical properties of aluminium–copper B206 alloys with iron and silicon additions [J]. International Journal of Cast Metals Research, 2012, 25(1): 15−25.

[21] LIU K, CAO X, CHEN X G. Tensile properties of Al−Cu 206 cast alloys with various iron contents [J]. Metallurgical and Materials Transactions A, 2014, 45(5): 2498−2507.

[22] LIN B, ZHANG W W. Evolution of iron-rich intermetallics and elevated temperature mechanical properties in gravity die cast 2A16 Al alloy [J]. International Journal of Cast Metals Research, 2018, 31(4): 222−229.

[23] FENG Z Q, YANG Y Q, HUANG B, LI M H, CHEN Y X, RU J G. Crystal substructures of the rotation-twinned $T$ ($Al_{20}Cu_2Mn_3$) phase in 2024 aluminum alloy [J]. Journal of Alloys and Compounds, 2014, 583: 445−451.

[24] LIU K, CAO X, CHEN X G. Solid-state transformation of iron-rich intermetallic phases in Al−Cu 206 cast alloys during solution heat treatment [J]. Metallurgical and Materials Transactions A, 2013, 44(8): 3494−3503.

[25] LIN B, ZHANG W W, ZHAO Y L, LI Y Y. Solid-state transformation of Fe-rich intermetallic phases in Al−5.0Cu−0.6Mn squeeze cast alloy with variable Fe contents during solution heat treatment [J]. Materials Characterization, 2015, 104: 124−131.

[26] LIU K, CHEN X G. Improvement in elevated-temperature properties of Al−13%Si piston alloys by dispersoid strengthening via Mn addition [J]. Journal of Materials Research, 2018: 33(20): 3430−3438.

[27] SHAHA S K, CZERWINSKI F, KASPRZAK W, FRIEDMAN J, CHEN D L. Ageing characteristics and high-temperature tensile properties of Al−Si−Cu−Mg alloys with micro-additions of Mo and Mn [J]. Materials Science and Engineering A, 2017, 684: 726−736.

[28] FARKOOSH A R, CHEN X G, PEKGULERYUZ M. Interaction between molybdenum and manganese to form effective dispersoids in an Al−Si−Cu−Mg alloy and their influence on creep resistance [J]. Materials Science and Engineering A, 2015, 627: 127−138.

[29] WANG E R, HUI X D, CHEN G L. Eutectic Al−Si−Cu−Fe−Mn alloys with enhanced mechanical properties at room and elevated temperature [J]. Materials & Design, 2011, 32(8−9): 4333−4340.

# Si 含量对 Al−6.5Cu−0.6Mn−0.5Fe 合金组织演变及力学性能的影响

许 锐[1]，林 波[1]，李浩宇[1]，肖华强[1]，赵俞亮[2]，张卫文[3]

1. 贵州大学 机械工程学院，贵阳 550025；
2. 东莞理工学院 机械工程学院，东莞 523808；
3. 华南理工大学 机械与汽车工程学院，广州 510640

**摘 要**：采用定量分析、扫描电镜、透射电镜和拉伸性能测试研究 Si 含量对高铁含量铝铜合金组织演变及力学性能的影响。结果表明：当 Si 含量低于 1.0%时，Al−6.5Cu−0.6Mn−0.5Fe 合金的常温力学性能稍有降低，这主要是由于组织演变的综合作用，包括纳米及 $\alpha$-Fe 相的增多，晶粒的粗化以及晶界处 $Al_2Cu$ 相的增多；当 Si 含量为 1.5%时，Al−6.5Cu−0.6Mn−0.5Fe 合金性能急剧下降，这主要是由于多余 Si 粒子的析出导致第二相产生偏聚。

**关键词**：铝铜合金；富铁金属间化合物；Si；拉伸性能

**(Edited by Bing YANG)**